

# We are IntechOpen, the world's leading publisher of Open Access books Built by scientists, for scientists

6,900

Open access books available

185,000

International authors and editors

200M

Downloads

Our authors are among the

154

Countries delivered to

TOP 1%

most cited scientists

12.2%

Contributors from top 500 universities



WEB OF SCIENCE™

Selection of our books indexed in the Book Citation Index  
in Web of Science™ Core Collection (BKCI)

Interested in publishing with us?  
Contact [book.department@intechopen.com](mailto:book.department@intechopen.com)

Numbers displayed above are based on latest data collected.  
For more information visit [www.intechopen.com](http://www.intechopen.com)



# Crystal Chemistry, Rietveld Analysis, Structural and Electrical Properties of Cobalt-Erbium Nano-Ferrites

*Edapalli Sumalatha, Dachepalli Ravinder, Nyathani Maramu, Shubha L.N., Butreddy Ravinder Reddy, Sadhana Katlakunta, Koteswari Gollapudi and Rajender Thota*

## Abstract

Synthesis of Cobalt-Erbium nano-ferrites with formulation  $\text{CoEr}_x\text{Fe}_{2-x}\text{O}_4$  ( $x = 0, 0.005, 0.010, 0.015, 0.020, 0.025, \text{ and } 0.030$ ) using technique of citrate-gel auto-combustion was done. Characterization of prepared powders was done by using XRD, EDAX, FESEM, AFM and FTIR Spectroscopy, DC resistivity properties respectively. XRD Rietveld Analysis, SEM, TEM and EDAX analysis were taken up in studying spectral, structural, magnetic and electrical properties. XRD pattern of CEF nano particles confirm single phase cubic spinal structure. The structural variables given by lattice constant ( $a$ ), lattice volume ( $v$ ), average crystallite size ( $D$ ) and X-ray density( $dx$ ), Bulk density ( $d$ ), porosity ( $p$ ), percentage of pore space ( $P\%$ ), surface area ( $s$ ), strain ( $\epsilon$ ), dislocation density ( $\delta$ ), along with ionic radii, bond length and hopping length were calculated. SEM and TEM results reveal homogeneous nature of particles accompanied by clusters having no impurity pickup. TEM analysis gives information about particle size of nanocrystalline ferrite while EDAX analysis confirm elemental composition. Emergence of two arch shaped frequency bands ( $\nu_1$  and  $\nu_2$ ) that represent vibrations at tetrahedral site (A) and octahedral site(B) was indicated by spectra of FTIR. The samples electrical resistivity (DC) was measured between  $30^\circ\text{C}$  - $600^\circ\text{C}$  with Two probe method. XRD Rietveld analysis confirm crystallite size lying between 20.84 nm–14.40 nm while SEM analysis indicate formation of agglomerates and TEM analysis indicate particle size ranging between 24 nm–16 nm. DC Electrical measurements indicate continuous decrease in resistivity with increasing temperature while increasing doping decreases curie temperature. The Magnetic parameters such as Saturation magnetization ( $M_s$ ), Remanent magnetization ( $M_r$ ), Coercivity ( $H_c$ ) and Squareness ratio ( $R = M_r/M_s$ ), Magnetic moment ( $n_B$ ) were altered by doping of  $\text{Er}^{+3}$  content in the increasing order ( $x = 0.00$  to  $0.030$ ). The increasing erbium content decreases magnetization thus converting the sample into soft magnetic material. Observations indicated strong dependence of magnetic properties on Erbium substitution and coercivity varies in accordance with anisotropy constant. Due to the presence of magnetic dipole Erbium substituted cobalt ferrites can be used in electromagnetic applications. The present study investigates

the effect of different compositions of  $\text{Er}^{3+}$  replaced for Fe on structural properties and electrical resistivity of cobalt ferrites.

**Keywords:** Electrical Resistivity Properties, Co-Er nano-Particles, TEM, XRD, FESEM, EDAX, AFM

## 1. Introduction

Vigorous research has been accomplished on the fundamental, technological and potential applications of nano-ferrites. Nanomaterials of spinel ferrite have several applications in technology that include magnetic diagnostics and drug delivery [1], potential applications that include high density magnetic information storage devices [2], ferrofluid technology [3], magneto caloric refrigeration [4], magnetic recording media, magnetostriction [5], magnetic sensors, microwave devices and electrical generators etc. Ferrites are also used for catalyst and electronic devices. Ferrites are insulators exhibiting various magnetic and electric properties such as low electrical conductivity, dielectric loss, magnetic loss, relative loss factor, moderate dielectric constant, high initial permeability and saturation magnetization. Low eddy current and high resistivity makes ferrites better choice than metals [6]. Doping and thermal changes during synthesis and processing of cobalt-ferrites alter the distribution of metal ions influencing their structure and magnetic properties [7]. Priya et al. [8] doped Al ions, with Cobalt ferrite nano particles. They observed that Al doped cobalt ferrite to be suitable for high frequency applications and magnetic memory devices. Nasir Amin et al. [9] synthesized yttrium substituted cadmium ferrites. They reported yttrium doped Cd nanoferrites can be used in high-frequency microwave absorbing devices. Salma et al. [10] synthesized ferrite series having formulation  $\text{SrYbyFe}_{2-y}\text{O}_4$  ( $y = 0.00$  to  $0.10$ ). They observed the dispersion of frequency of ferrites is responsible for the natural magnetic resonance phenomenon and the domain wall pinning. As per the literature net magnetic moment of lanthanide series elements/ions depend on f-orbital electron number in which  $\text{Er}^{+3}$  is of small size (89 pm) with large magnetic moment ( $7 \mu\text{B}$ ) [11]. Magnetic anisotropy of cobalt ferrites if doped get influenced by the existence of  $\text{Er}^{+3}$  because of strength in spin-orbit coupling. The present work reports the preparation and characterization of erbium doped cobalt ferrites combined by Citrate-gel auto combustion. The studies of  $\text{CoEr}_x\text{Fe}_{2-x}\text{O}_4$  with cobalt content  $x$  values ranging between 0.000 to 0.030 with step increase of  $x = 0.005$  was reported. The crystallite size decrease with increasing erbium content indicating increase in surface area of the particle making it a good adsorbent. These adsorbents can be used in gas sensors and waste water treatment etc.

## 2. Experimental procedure

Synthesis of Cobalt-Erbium nano-ferrites with citrate-gel auto combustion technique was taken up with starting materials Cobalt Nitrate ( $\text{Co}(\text{NO}_3)_2 \cdot 6\text{H}_2\text{O}$ ), Ferricnitrate ( $\text{Fe}(\text{NO}_3)_3 \cdot 9\text{H}_2\text{O}$ ), Erbium Nitrate ( $\text{Er}(\text{NO}_3)_3 \cdot 6\text{H}_2\text{O}$ ), Citric Acid ( $\text{C}_6\text{H}_8\text{O}_7 \cdot \text{H}_2\text{O}$ ) and Ammonia solution ( $\text{NH}_3$ ) of 99.9% purity after weighing as per stoichiometric ratio. Later liquification of metal nitrates in distilled water was done and the mixture was stirred at 300 rpm for one hour to obtain a clear homogeneous solution. Next citric acid in aqueous form and metal nitrate was maintained in 1:3 ratio for all samples. Now, ammonia solution was added drop by drop to maintain  $\text{pH} = 7$ . This solution on stirring was heated at  $100^\circ\text{C}$  temperature for ten to twelve hours to form a viscous gel. The water contained in the mixture gets evaporated slowly to form dry gel generating internal combustion to form a black colored

desired sample. This sample was manually grinded and subjected to calcinations at 500°C in furnace for 4 hours. The step by step procedure for the synthesis of crystal ferrites is shown in the form of flow chart in **Figure 1**. Pellet was prepared with KBr hydraulic press (Model: M-15) in 2–3 mm thickness and 10 mm diameter size

Later these samples in pellet or powder form were used to characterize the material. Structural properties were analyzed with XRD (Bruker, CuK $\alpha$ ,  $\lambda = 0.15406$  nm), TEM (Model JEOL 2100F, Japan), Field-emission Scanning Electron Microscope (JEOL JSM-7600 F, Japan), Energy Dispersive X-ray Analyzer (EDAX) and, Atomic Force Microscopy (AFM: VEECO, USA). Two probe method was used to study electric properties.

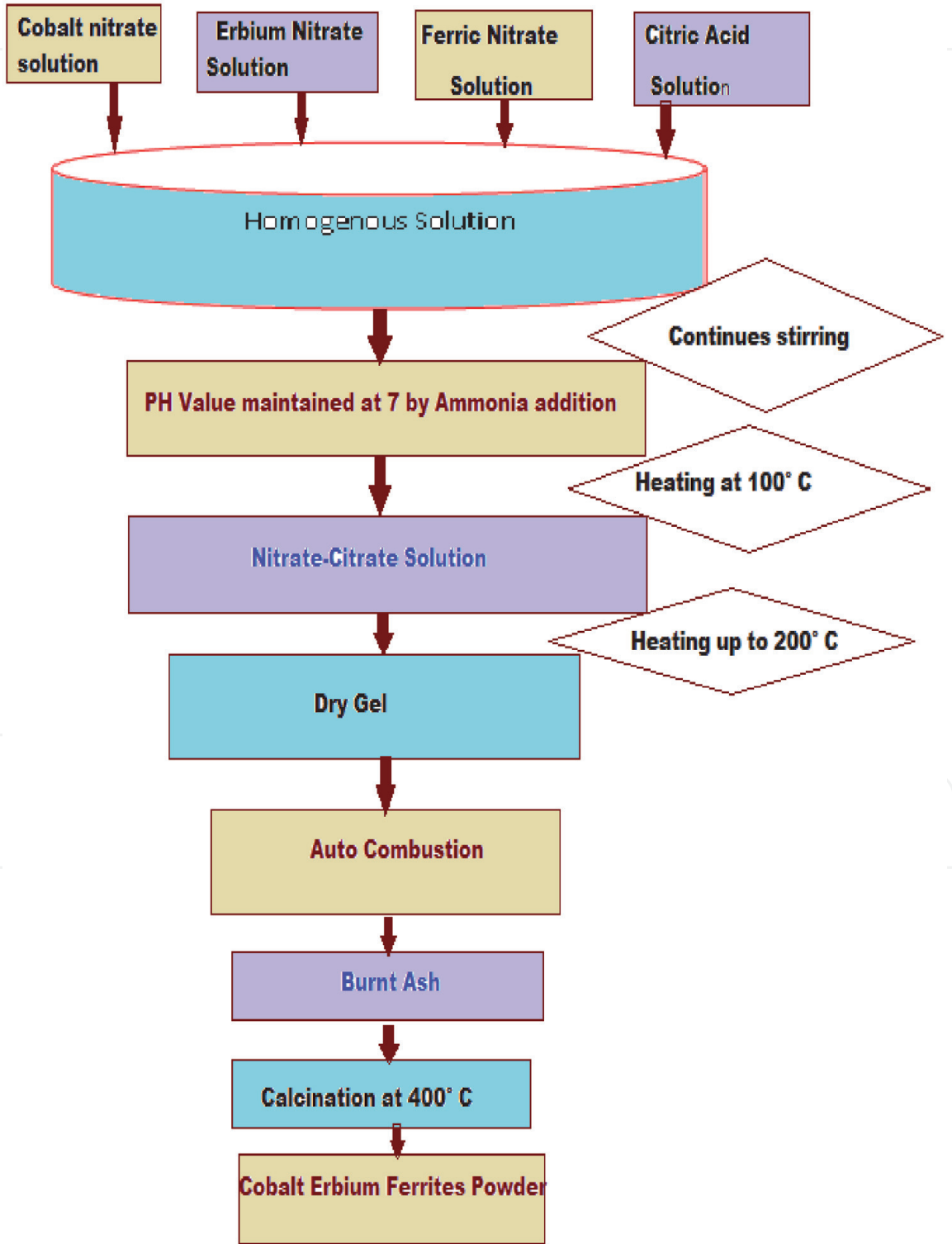


**Figure 1.**  
Flow chart for the synthesis of cobalt-erbium ferrite using citrate-gel auto combustion technique.

### 3. Results and discussion

#### 3.1 XRD analysis

Figure 2 displays the XRD Rietveld Refinement corresponding to samples of  $\text{CoEr}_x\text{Fe}_{2-x}\text{O}_4$  with values of  $x$  between 0.00 to 0.030 ( $x$  = incremented by 0.005).

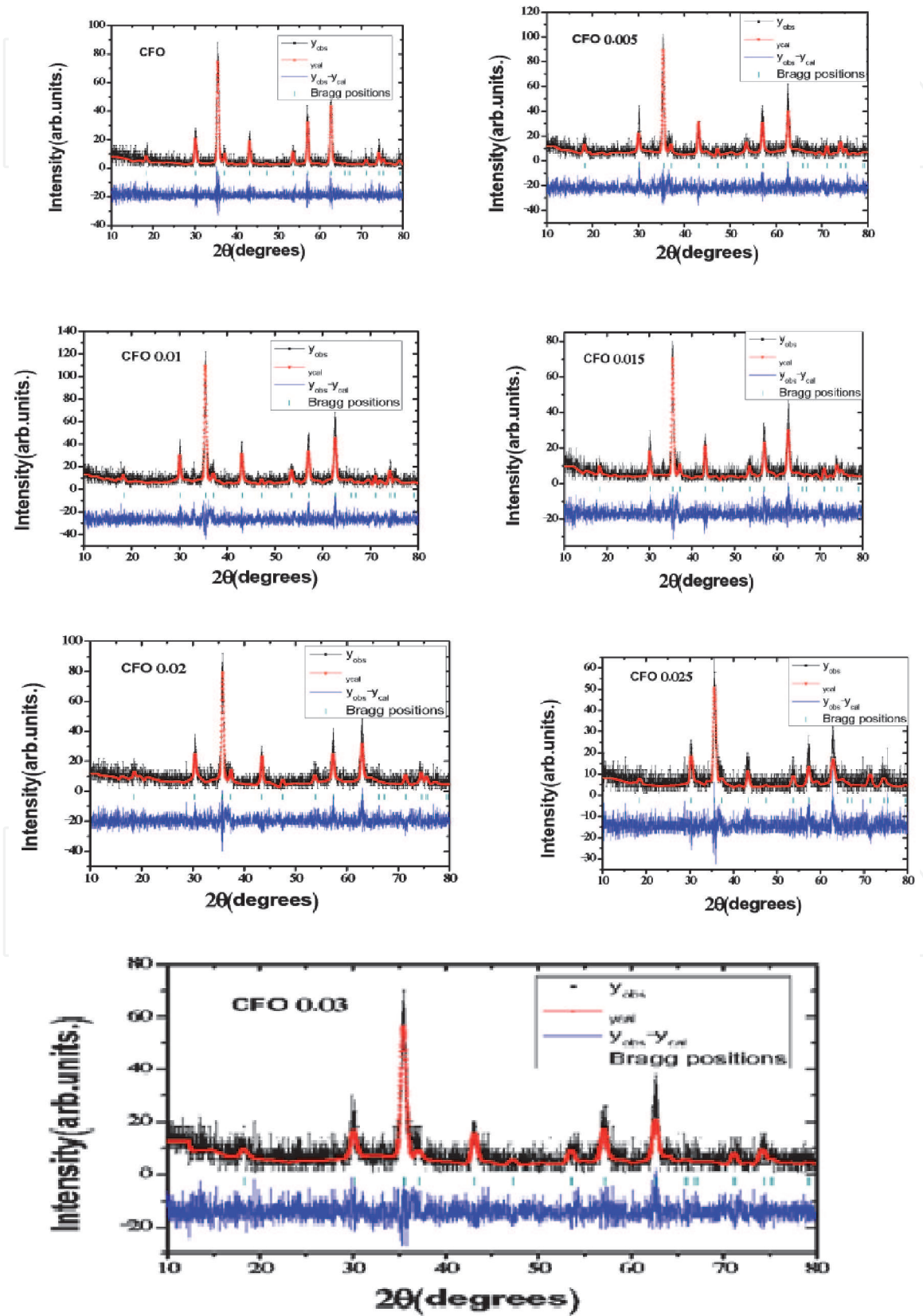


Figure 2.  
XRD Rietveld refinement pattern of Er-substituted  $\text{CoFe}_2\text{O}_4$ .



It is observed that the peaks analogous to diffraction planes [111], [320], [311], [400], [511] and [440] match with usual data (JCPDS card no. 022-1086) confirming FCC cubic spinel structure for samples investigated [12, 13]. **Figure 3** shows shift in XRD peaks towards left hand side with increasing concentration of  $\text{Er}^{+3}$  ions in  $\text{CoFe}_2\text{O}_4$  particles in concurrence with ‘a’ value. **Table 1** lists different parameters of XRD calculated for  $\text{CoEr}_x\text{Fe}_{2-x}\text{O}_4$  nanoparticles. The values of ‘a’ were calculated from the equation given [14].

$$a = d * (h^2 + k^2 + l^2)^{1/2} \tag{1}$$

where cell constant is given by ‘a’, inter planer spacing calculated from Bragg’s equation ( $2 \text{d} \sin \theta = n\lambda$ ) is denoted by ‘d’ and miller indices are done by ‘h,k,l’.

It was reported that, low concentration RE (rare earth) doping in spinel ferrite experience phase separation and grain boundary diffusion giving rise to precipitation of additional crystalline phases like hematite ( $\alpha\text{-Fe}_2\text{O}_3$ ), metal monoxides and orthoferrites ( $\text{REFeO}_3$ ) [15–17]. Hence in case of rare earth doped ferrites,  $\text{Er}^{+3}$  doped CFO having no impurity phase ( $x \leq 0.010$ ) is exceptional and is because of auto-combustion. Induced effect due to substitution of erbium on the structure reflects two main observations given by decrease in size of crystal and increase in lattice constant both on small scale. The value of lattice constant slightly enhanced between 8.361 Å to 8.398 Å for  $x = 0.000$  to  $x = 0.030$  as per Law of Vegard [18]. Scherrer formula was used to calculate the crystallite size given by [19]:

$$L = \frac{0.9 * \lambda}{\beta \cos \theta} \tag{2}$$

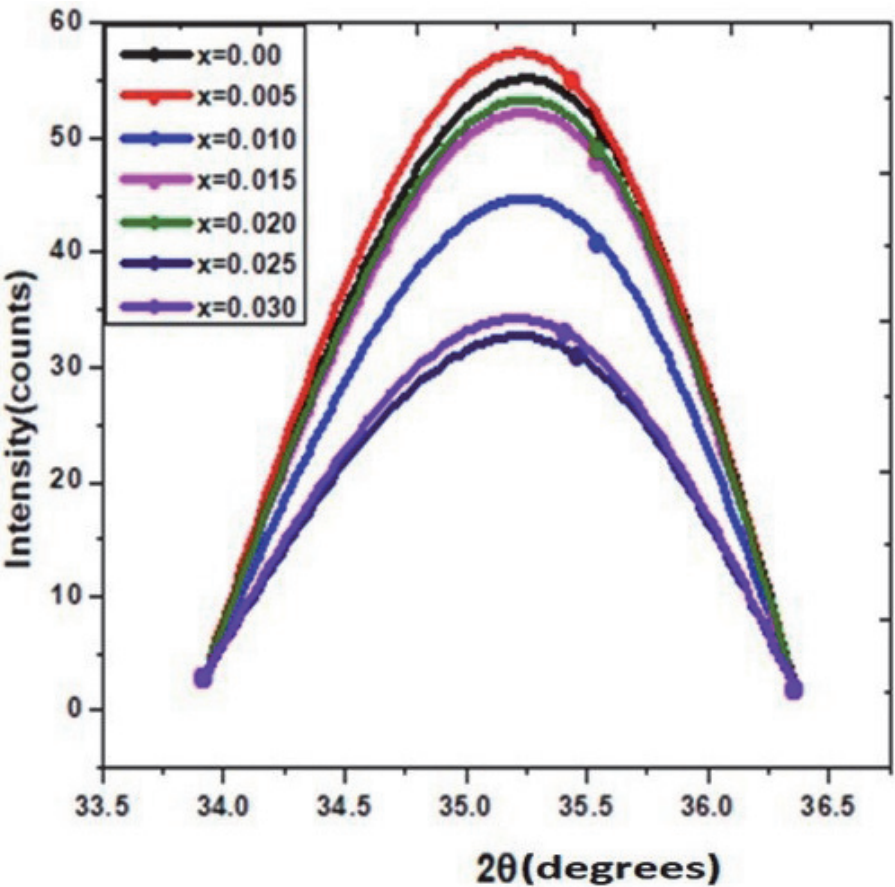


**Figure 3.**  
XRD pattern of Er-substituted  $\text{CoFe}_2\text{O}_4$  and shifting of peaks.

Compositions	Cell constant (Å)	Cell Volume V(Å <sup>3</sup> )	Crystallite Size (nm)	X-ray density (dx) (gcm <sup>-3</sup> )	Bulk density(d) (gcm <sup>-3</sup> )	Porosity P (%)	Surface area(s) (m <sup>2</sup> /gm)	Packing factor(P)	Strain (ε) x10 <sup>-3</sup>	Dis location density (δ)x10 <sup>-4</sup>
CoFe <sub>2</sub> O <sub>4</sub>	8.361	V = 584.48	20.84	5.3344	3.2113	39.8001	89.61	8.26	2.3	1.9
CoEr <sub>0.005</sub> Fe <sub>1.995</sub> O <sub>4</sub>	8.367	V = 585.74	20.43	5.3356	3.2120	39.8005	91.39	8.09	2.3	2.0
CoEr <sub>0.010</sub> Fe <sub>1.990</sub> O <sub>4</sub>	8.373	V = 587.00	19.19	5.3367	3.2127	39.7998	97.34	7.60	2.7	2.5
CoEr <sub>0.015</sub> Fe <sub>1.985</sub> O <sub>4</sub>	8.379	V = 588.26	19.02	5.3379	3.2134	39.8003	98.18	7.52	2.7	2.5
CoEr <sub>0.020</sub> Fe <sub>1.980</sub> O <sub>4</sub>	8.386	V = 589.74	17.73	5.3370	3.2129	39.7995	105.38	7.01	3.1	3.2
CoEr <sub>0.025</sub> Fe <sub>1.975</sub> O <sub>4</sub>	8.392	V = 591.01	15.56	5.3381	3.2135	39.8006	119.99	6.14	4.1	4.7
CoEr <sub>0.030</sub> Fe <sub>1.970</sub> O <sub>4</sub>	8.398	V = 592.28	14.40	5.3392	3.2141	39.8018	132.58	5.68	4.8	5.9

**Table 1.**  
*Structural parameters of the prepared Co-Er nano ferrite sample.*

where ' $\lambda$ ' = wavelength of x ray, ' $\beta$ ' = peak width at half maximum height and constant ' $K$ ' = 0.9. The data related to intense peak (311) was used in estimating size (L). The results indicated reduction in size of crystallite from 20.84nm to 14.40 nm (for  $x = 0.0$  to 0.030). Further, the high intense peak (311) shifts towards the lower angle with increasing values of  $x$  (**Figure 3**). **Table 1** lists the physical parameters obtained from XRD which indicated increase in lattice constant of Co-Fe-Er spinel lattice which might be due to replacement of 8 small  $\text{Co}^{2+}$  and  $\text{Fe}^{3+}$  ions with big  $\text{Er}^{3+}$  ions. Huge difference in radii of these three ions induce strain during formation of lattice and diffusion processes. Requirement of more energy in absorbing  $\text{RE}^{3+}$  ions with more radii while replacing  $\text{Fe}^{3+}$  to form RE-O bond decreases crystallization energy and leads to particles of small size. Earlier literature reported similar results on RE-ion substituted cobalt ferrite [20–23]. From **Table 2**, EDAX confirmed the effect of incorporating  $\text{Er}^{3+}$  into CFO and stoichiometric amount of O, Fe, Co, and Er atoms. Therefore, XRD results are liable for expansion of unit cell due to larger  $\text{Er}^{3+}$  ion doping in CFO. Calculation of X-ray density ( $D_x$ ) was done using [24]:

$$d_x = \frac{8 * M}{Na^3} \tag{3}$$

Here  
'M' = composition molecular weight.  
'N' = Avogadro's number.  
'a' = lattice constant.

X-ray density value is found to increase from 5.3344 gm/cm<sup>3</sup> to 5.3392 gm/cm<sup>3</sup> ( $x = 0.00$  to  $x = 0.030$ ) with increasing  $\text{Er}^{3+}$  content. The bulk density increased from 3.2113 to 3.2141 ( $x = 0.00$  to  $x = 0.030$ ). At the same time,  $\text{CoFe}_{2-x}\text{Er}_x\text{O}_4$  ceramics having more Er content ( $x = 0.015$ ) exhibited lower  $\text{ErFeO}_3$  orthoferrite amount along with primary spinel ferrite phase. Cobalt ferrite in inverse spinel form has tetrahedral site occupied by half of  $\text{Fe}^{+3}$  while the remaining half of  $\text{Fe}^{+3}$  and  $\text{Co}^{-2}$  occupy octahedral sites [25]. Any change in site occupation of  $\text{Fe}^{+3}$  and  $\text{Co}^{-2}$  might be because of preparation technique and affect cell constant. Bulk densities were found from the relation [26].

$$d = \frac{m}{\pi r^2 h} \tag{4}$$

where pellets mass, thickness and radius are given by ' $m$ ', ' $h$ ' and ' $r$ '. Bulk densities exhibit inhomogeneous behavior due to pellets variable thickness and mass. The values of porosity in percentage were found using the relation.

Composition	$d_{A-A}$	$d_{B-B}$	$d_{A-B}$	$d_{A-OA}$	$d_{A-OB}$
$\text{CoFe}_2\text{O}_4$	3.620	2.956	3.466	1.926	2.025
$\text{CoEr}_{0.005}\text{Fe}_{1.995}\text{O}_4$	3.622	2.958	3.468	1.927	2.026
$\text{CoEr}_{0.010}\text{Fe}_{1.990}\text{O}_4$	3.625	2.960	3.471	1.928	2.027
$\text{CoEr}_{0.015}\text{Fe}_{1.985}\text{O}_4$	3.628	2.962	3.473	1.930	2.029
$\text{CoEr}_{0.020}\text{Fe}_{1.980}\text{O}_4$	3.631	2.964	3.476	1.931	2.031
$\text{CoEr}_{0.025}\text{Fe}_{1.975}\text{O}_4$	3.633	2.966	3.479	1.933	2.032
$\text{CoEr}_{0.030}\text{Fe}_{1.970}\text{O}_4$	3.636	2.969	3.481	1.934	2.033

**Table 2.**  
Summarizes different bond lengths of A, B sites due to  $\text{Er}^{+3}$  ion doping in spinel lattice.



$$P\% = (1 - d/d_x) \times 100 \quad (5)$$

Here  $d$  and  $d_x$  are apparent and experimental densities. Surface area was calculated by using the Eq. (16).

$$S = \frac{6000}{D * d} \quad (6)$$

Here,  $S$  = area of surface,  $D$  = crystallite size,  $d$  = Bulk density. Strain was calculated by using the following Equation [27].

$$\text{Strain } (\epsilon) = 1/D^2 \quad (7)$$

Dislocation Density calculated by using following equation

$$\text{Dislocation density } (\delta) = 15\epsilon/aD \quad (8)$$

Here  $\epsilon$  is strain,  $a$  is lattice constant,  $D$  is crystallite size. Packing factor is calculated by using following equation

$$P = \frac{Lnm}{d} \quad (9)$$

Here  $L$  is crystallite size,  $d$  is inter planner spacing.

Cationic distributions that depend on factors like synthesis, total energy and thermal history are useful in understanding spinel ferrites behavior (electric and magnetic). Cationic calculations play important role in this regard. Average ionic radii of A, B sites were calculated from Stanley's equations:

$$r_A = [u - 1/4]a \times (3)^{0.5} - R_o \quad (10)$$

$$r_B = (5/8 - u)a - R_o \quad (11)$$

Here  $R_o$  is the radius of the oxygen ion (1.35 Å), 'u' is the oxygen parameter whose ideal value is 0.375Å and experimental value is 0.383Å.

Bonding lengths and hopping lengths are calculated by using following formulas [28].

Bonding lengths: Hopping lengths:

$$d_{A-A} = \frac{a}{4} \times (3)^{0.5} \quad (12)$$

$$d_{B-B} = \frac{a}{4} \times (2)^{0.5}a \quad (13)$$

$$d_{A-B} = \frac{a}{8} \times (11)^{0.5} \quad (14)$$

$$d_{A-OA} = a \left( u - \frac{1}{4} \right) * (3)^{0.5} \quad (15)$$

$$d_{B-OB} = a \left\{ 2 \left( u - \frac{3}{8} \right)^2 + \left( \frac{5}{8} - u \right)^2 \right\}^{0.5} \quad (16)$$

$$L_A = \frac{\sqrt{3}}{4} \times a \quad (17)$$

$$L_B = \frac{\sqrt{2}}{4} \times a \quad (18)$$

The difference in ‘u’ value in comparison with its ideal value on substituting  $\text{Er}^{+3}$  ions has been explained with  $r_A$  values. Increasing  $r_A$  values increase ‘u’ showing distortion in  $\text{CoFe}_2\text{O}_4$  spinel lattice. Calculated values of ionic radii for B-sites are slightly higher than A-site because more  $\text{Er}^{+3}$  ions reside at B-site than A-site. Hopping length is the gap between magnetic ions at A, B sites. The hopping lengths between magnetic ions at A, B sites are denoted by  $L_A$  and  $L_B$  whose values reduce with addition of  $\text{Er}^{+3}$  content and is consistent with variation in lattice constant on adding  $\text{Er}^{+3}$  ions. The determined values from the formulas (10), (11), (17) and (18) are listed in **Table 1**.

By using the relations below structural parameters associated with A, B sites are calculated. Magnetic interactions and their strengths among AA, BB and AB sites mainly depend on bond length and bond angle existing between positive and negative ions. Increase in bond angle increases magnetic interaction strength while it reduces with increasing bond length as the strength has direct relation with bond angle and inverse relation with bond length. **Table 3** summarizes different bond lengths of A, B sites ( $d_{A-A}$ ,  $d_{B-B}$ ,  $d_{A-B}$ ,  $d_{A-OA}$ ,  $d_{B-OB}$ ) which depict an increase in bond lengths of tetrahedral and octahedral sites which is due to  $\text{Er}^{+3}$  ion doping in spinel lattice which might be due to larger  $\text{Er}^{+3}$  ions replacing smaller  $\text{Fe}^{+3}$  ions.

3.2 EDAX analysis

**Figure 4** displays the EDAX spectrums that analyzed elemental and atomic percentages of  $\text{CoFe}_{2-x}\text{Er}_x\text{O}_4$  nanoparticles for  $x = 0.0, 0.005, 0.010, 0.015, 0.020, 0.025$  and  $0.030$ . It confirmed the presence of Co, O, Fe and Er. Er peak confirms Erbium substitution in the  $\text{Fe}_{2-x}$  lattice.

**Table 2** summarizes atomic percentages of individual in  $\text{CoFe}_{2-x}\text{Er}_x\text{O}_4$  nanoparticles. EDAX confirmed the effect of incorporating  $\text{Er}^{3+}$  into CFO and stoichiometric amount of O, Fe, Co, and Er atoms.

3.3 Field emission scanning Electron microscopy (FE-SEM)

**Figure 5** shows studies on surface morphology of ferrite powders with the help of FE-SEM. The nature of ferrite particle in the samples is uniform indicating fine form of agglomeration and grain growth. Agglomerate formation specifies strong magnetic nature of erbium doped ferrites. These studies also confirm microstructure changes on doping  $\text{Er}^{+3}$ . A close look at these microstructures indicate improvement in microstructure and spherical shaped grains in all samples. Apart from this Erbium doping increases percentage of porosity in small range between 39.8001to 39.8018 illustrating individual grains and grain boundaries are separated.

Composition(x)	Co	Fe	Er	O
X = 0.000	12.40	34.43	0.000	26.86
X = 0.005	12.37	34.27	0.094	26.80
X = 0.010	12.34	34.10	0.18	26.74
X = 0.015	12.31	33.93	0.28	26.67
X = 0.020	12.28	33.77	0.37	26.61
X = 0.025	12.25	33.60	0.46	26.55
X = 0.030	12.23	33.44	0.55	26.49

**Table 3.**  
summarizes atomic percentages of  $\text{CoFe}_{2-x}\text{Er}_x\text{O}_4$  nanoparticles for  $x = 0.0, 0.005, 0.010, 0.015, 0.020, 0.025$  and  $0.030$ .

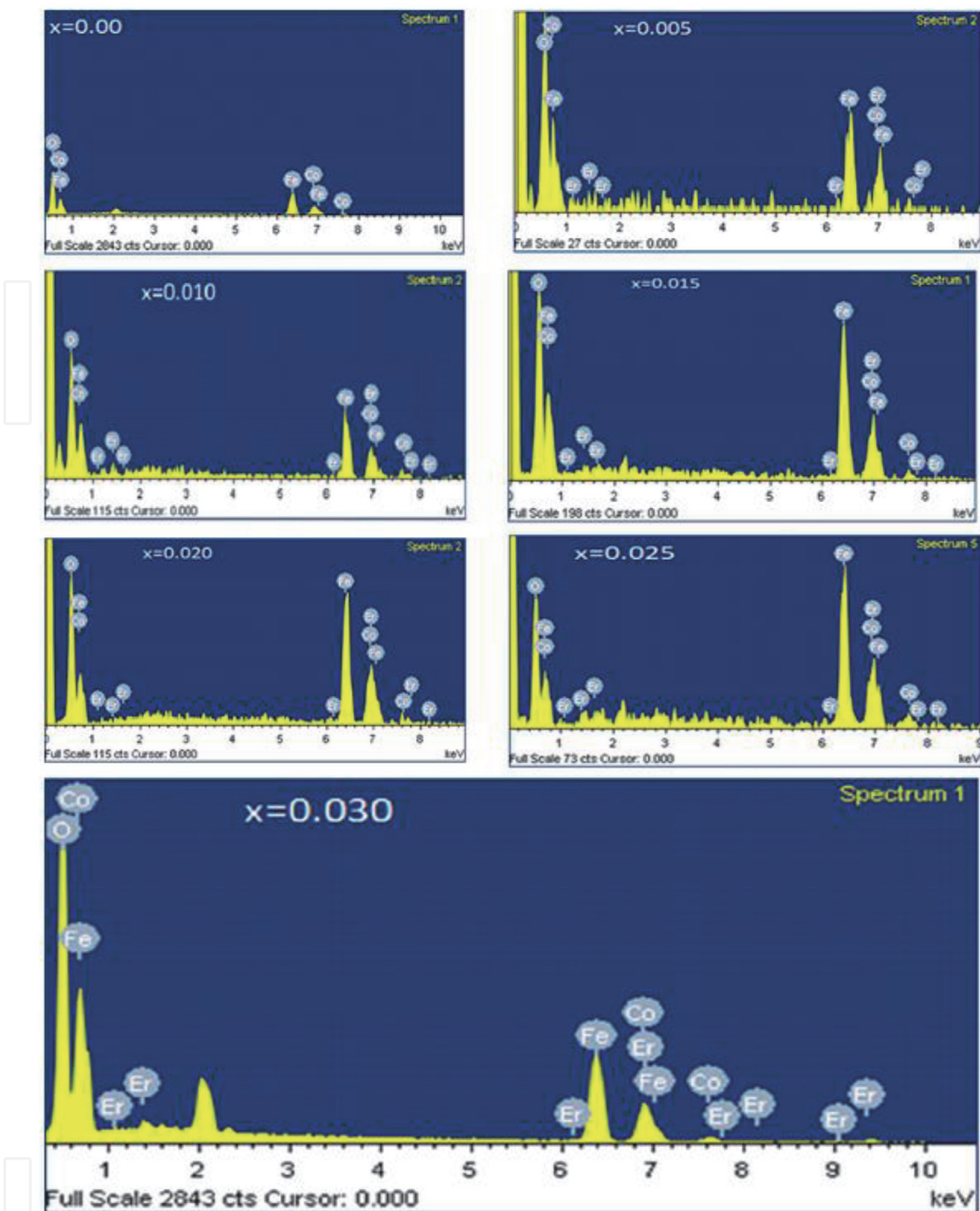


**Figure 4.**  
Displays the EDAX spectrums that of  $\text{CoFe}_{2-x}\text{Er}_x\text{O}_4$  nanoparticles.

### 3.4 Atomic force microscopy (AFM)

AFM was used to characterize the surface roughness of  $\text{CoEr}_x\text{Fe}_{2-x}\text{O}_4$  nano ferrite samples of the synthesized nanoparticles. The three-dimensional arrangement of the spherical nanoparticles and diameter are shown in **Figure 6**. The surface roughness increased when the coercivity increases, but in this work all the parameters crystallite size, saturation magnetization, remanent magnetization, coercivity decreased with the increasing of Er dopant from  $x = 0.00$  to  $0.030$  in the cobalt ferrite. In view of the above, the largest surface roughness is observed for  $x = 0.0$  sample and the lowest surface roughness is obtained for Er ( $x = 0.030$ ) doped samples. This indicates that the surface activity of  $x = 0.0$  ferrite has higher values compared to the range  $x = 0.005$ – $0.030$  ferrite samples. The largest surface roughness is observed for  $x = 0.0$  sample that is, it behaves like hard ferrite and the



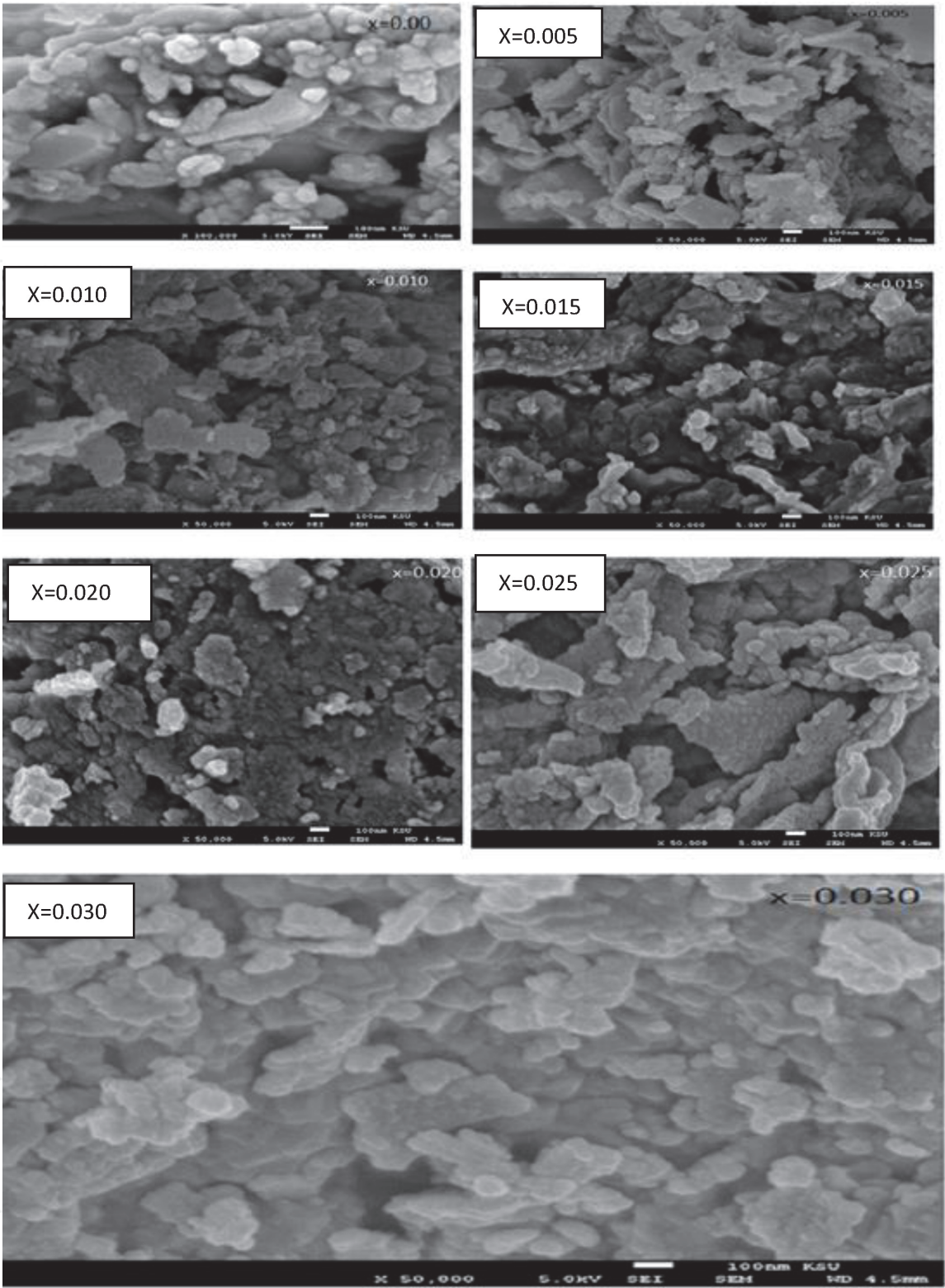


**Figure 5.**  
*Displays FE-SEM images of  $\text{CoFe}_{2-x}\text{Er}_x\text{O}_4$  nanoparticles.*

lowest surface roughness is obtained for Er ( $x = 0.030$ ) doped samples. That is, it behaves like soft ferrite, hereby the ferrite is transformed from hard ferrite to soft ferrite due to the doping of Er content.

### 3.5 TEM analysis

Phase structure and morphology studies for the investigating synthesized samples were taken up through TEM analysis. **Figure 7** shows the TEM images and their

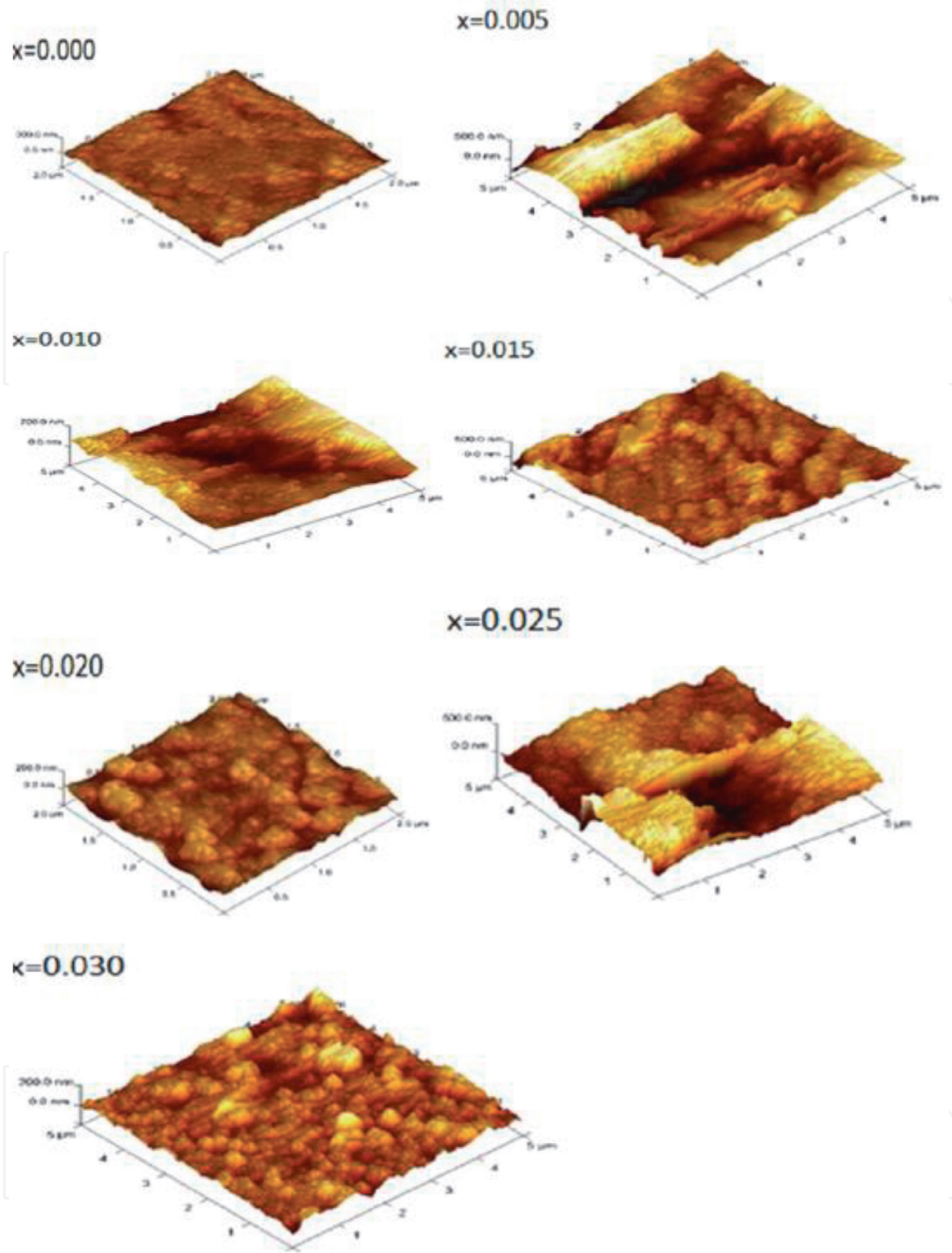


**Figure 6.**  
AFM Micrographs of  $\text{CoFe}_2\text{O}_4$  ( $x = 0.000$ ) and  $\text{CoFe}_{2-x}\text{Er}_x\text{O}_4$  ( $x = 0.005$  to  $0.030$ ).

respective SAED images with particle size distribution chart of the samples got  $x = 0.0, 0.005, 0.01, 0.015, 0.02, 0.025$  and  $0.03$  respectively. TEM and SAED images demonstrated spherical shape and less thickness for majority of the nanoparticles along with few elongated particles. Observation of TEM images confirm well distanced particles for lower concentration of  $\text{Er}^{+3}$  ions and increase in  $\text{Er}^{+3}$  ion substitution leads to agglomeration of particles because of magnetic nanoparticle interaction which makes the particles to be stacked on top of each other. The particle size measured from TEM images are in the range  $16\text{nm}$ – $24\text{ nm}$ .



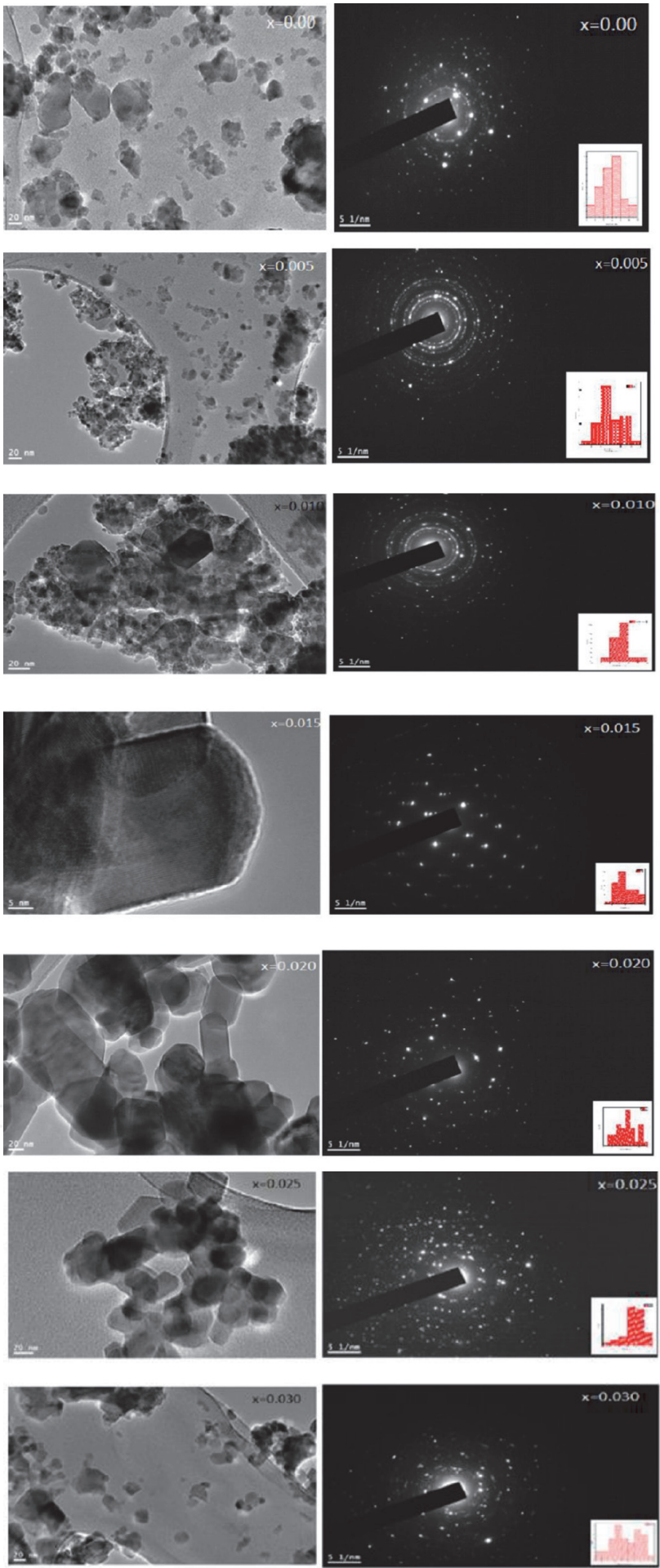


**Figure 7.**  
TEM/SAED images of  $\text{CoFe}_2\text{O}_4$  ( $x = 0.000$ ) and  $\text{CoFe}_{2-x}\text{Er}_x\text{O}_4$  ( $x = 0.005$  to  $0.030$ ).

3.6 FTIR analysis

FTIR (Fourier Transform Infrared) spectroscopy is a very useful technique that estimates cationic redistribution at A and B sites of spinel ferrites. FTIR spectra for samples between 400 cm<sup>-1</sup> and 1000 cm<sup>-1</sup> was displayed by **Figure 8** in which two important broad bands (1 in the range 500 cm<sup>-1</sup> – 600 cm<sup>-1</sup> and 2 in the range 400cm<sup>-1</sup> – 500 cm<sup>-1</sup>) were observed. As per Waldron suggestion intrinsic vibrations of M–O complexes was shown by band 1 at site A site and band 2 at site B. This difference between 1 and 2 was because of variation in bond length of Fe<sup>+3</sup>-O<sup>-2</sup> at A, B sites [29]. Observations indicate shift in octahedral (2) and tetrahedral (1) bands towards higher frequency with the addition of Er<sup>+3</sup> ions due to bond length variation, expansion in A, B sites and cation migration between two sites. The residency of Er<sup>+3</sup> ions at B-site was also confirmed. FT-IR spectra of CoFe<sub>2</sub>O<sub>4</sub> (x = 0.00) and CoEr<sub>x</sub>Fe<sub>2-x</sub>O<sub>4</sub> (x = 0.005 to 0.030) nanoparticles are shown in **Figure 8**. The values of force constant at tetrahedral and octahedral (Ft&Fo) sites were determined using the formulas below [30] whose values are listed in **Table 4**.

$$F_t = 4\pi^2 c^2 \nu_1^2 u \tag{19}$$

$$F_o = 4\pi^2 c^2 \nu_2^2 u \tag{20}$$

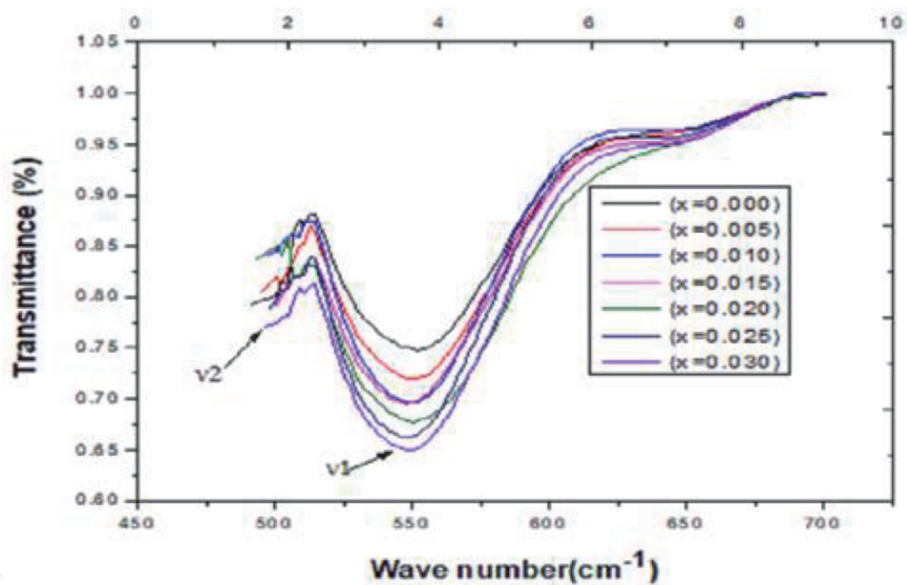


**Figure 8.** FTIR spectra of CoFe<sub>2</sub>O<sub>4</sub> (x = 0.000) and CoFe<sub>2-x</sub>Er<sub>x</sub>O<sub>4</sub> (x = 0.005 to 0.030).

Compositions	Wave number $\nu_1(\text{cm}^{-1})$	Wave number $\nu_2(\text{cm}^{-1})$	FT×105 (dynes/cm)	FO×105 (dynes/cm)
CoFe <sub>2</sub> O <sub>4</sub>	548	488	2.18	1.72
CoEr <sub>0.005</sub> Fe <sub>1.995</sub> O <sub>4</sub>	550	490	2.20	1.74
CoEr <sub>0.010</sub> Fe <sub>1.990</sub> O <sub>4</sub>	556	492	2.25	1.76
CoEr <sub>0.015</sub> Fe <sub>1.985</sub> O <sub>4</sub>	564	494	2.31	1.77
CoEr <sub>0.020</sub> Fe <sub>1.980</sub> O <sub>4</sub>	570	495	2.36	1.78
CoEr <sub>0.025</sub> Fe <sub>1.975</sub> O <sub>4</sub>	572	496	2.38	1.79
CoEr <sub>0.030</sub> Fe <sub>1.970</sub> O <sub>4</sub>	570	498	2.36	1.80

**Table 4.** Summarizes FTIR modes( $\nu_1, \nu_2$ ) and force constants ( $F_T, F_O$ ) of CoFe<sub>2-x</sub>Er<sub>x</sub>O<sub>4</sub> nano particles.

where vibrational frequencies of A, B sites are denoted by  $\nu_1, \nu_2$ , reduced mass of  $\text{Fe}^{3+}$  and  $\text{O}^{2-}$  ions is  $u$ , speed of light =  $c$ . Because of changes in bond lengths of  $\text{Fe}^{3+}$  and  $\text{O}^{2-}$  ions at A, B sites variation in values of force constant was determined.

### 3.7 Resistivity analysis

Resistivity figures signify distinct  $\log \rho$  vs.  $1000/T$  for various compositions of  $\text{CoFe}_{2-x}\text{Er}_x\text{O}_4$ . Resistivity reducing while increasing temperature, this behavior indicates that the semiconducting behavior of the prepared samples. Mobility of charge carriers (drift) reduces resistivity with temperature. Enhancement in temperature boosts enough energy to improve charge carriers hopping from one cationic site to other. The  $\mu D$  is growing up with the raise of  $\text{Er}^{+3}$  content the low drift mobility means temperature has not supplied sufficient potential to develop charge carriers to click from one site to another. Enrichment in  $\mu D$  with the boost of  $\text{Er}^{+3}$  contents advocate the enhancement of hopping from one cationic site to other for all nano ferrites synthesized particles. DC resistivity and drift mobility have inverse relation with each other. Observed resistivity figures indicated increase in resistivity initially for  $x = 0.000$  and later decreases with increasing Er for  $x = 0.005$  to  $0.030$ . It is evident that all specimens contain a fixed quantity of Co. Resistivity vs. temperature curves of Er-substituted  $\text{CoFe}_2\text{O}_4$  nanoparticles are shown in **Figure 9**. The resistivity is calculated from the following formula.

$$\rho = \frac{RA}{l} \tag{21}$$

Here R is the resistance, A is area of the pellet, l is length of the pellet.

### 3.8 Magnetic properties

M-H curves (Hysteresis Loops) are plots drawn between magnetization (M) and applied field (H) which helps us in analyzing magnetic response and magnetic parameters of ferrites under investigation. The M-H loops of all nanoparticles, that is  $\text{CoEr}_x\text{Fe}_{2-x}\text{O}_4$  ( $x = 0.00-0.030$ ) heated at  $500^\circ\text{C}$  are displayed in **Figure 10**. The

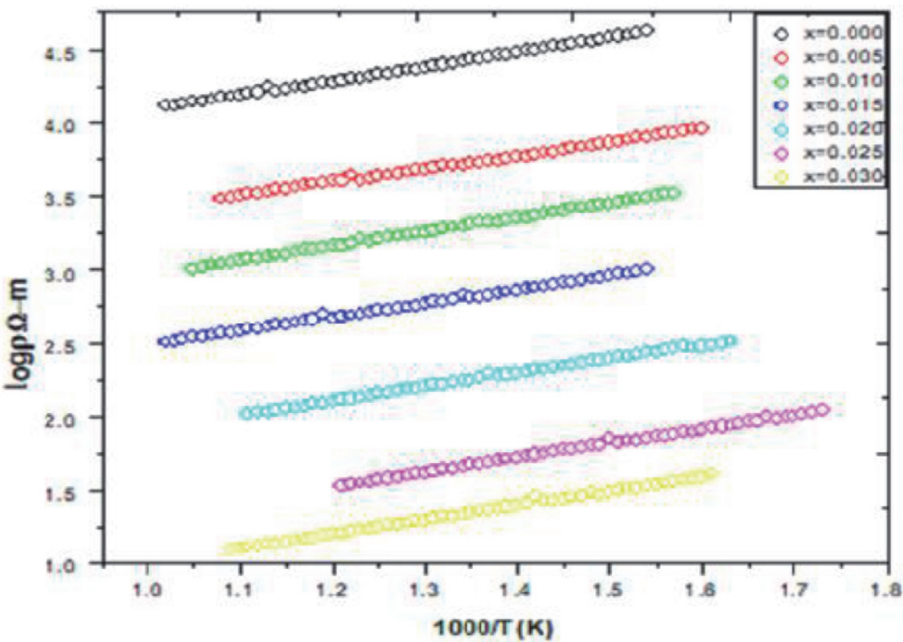


**Figure 9.**  
Resistivity vs. temperature curves of Er-substituted  $\text{CoFe}_2\text{O}_4$ .

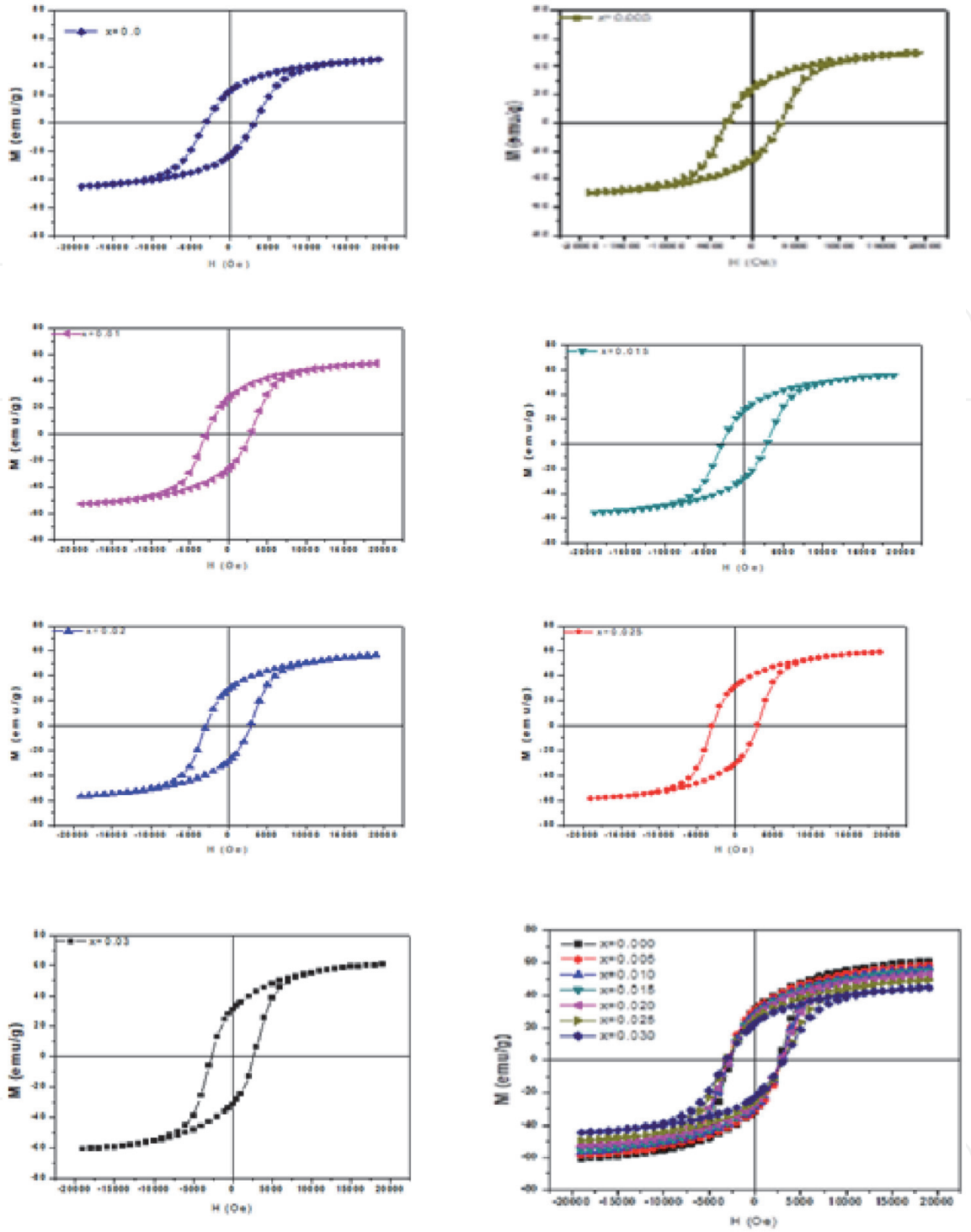


**Figure 10.**  
The magnetic hysteresis curves of Er-substituted  $\text{CoFe}_2\text{O}_4$  nano particles at room temperature.

measured magnetic parameters are displayed in **Table 5**. The Magnetic parameters such as Saturation magnetization ( $M_s$ ), Remanent magnetization ( $M_r$ ), Coercivity ( $H_c$ ) and Squareness ratio ( $R = M_r / M_s$ ), Magnetic moment ( $n_B$ ) were altered by doping of  $\text{Er}^{+3}$  content in the increasing order ( $x = 0.00$  to  $0.030$ ). Generally, dopant type, concentration and morphology will affect magnetic properties of soft ferrite sample. At the same time variation in magnetic parameters was seen due to microstructure with noting of higher saturation magnetization with higher grain size [31, 32]. **Table 5** indicate high saturation magnetization and coercivity due to large grain size in  $\text{CoFe}_2\text{O}_4$  ferrites as depicted by the hysteresis loop in **Figure 10**.  $M_s$  value decreased from  $60 \text{ emu/g}$  to  $44 \text{ emu/g}$  with decrease in grain size due to increased Er content in cobalt ferrite which may be due to increase of erbium



Composition	Lattice parameter (a)	Crystallite Size (nm)	Hc (c)	Ms (emu/g)	Mr (emu/g)	R=Mr/Ms	K (erg/Oe)	Magnetic moment (μB/f.u)
CoFe <sub>2</sub> O <sub>4</sub>	8.361	20.34	2998	60.6739	31.19	0.5141	189,479.783	2.5488
CoEr <sub>0.005</sub> Fe <sub>1.995</sub> O <sub>4</sub>	8.392	20.43	2997	58.7486	31.07	0.5289	183,405.941	2.4738
CoEr <sub>0.010</sub> Fe <sub>1.990</sub> O <sub>4</sub>	8.407	19.19	2996	56.9560	28.86	0.5067	177,750.433	2.4040
CoEr <sub>0.015</sub> Fe <sub>1.985</sub> O <sub>4</sub>	8.367	19.02	2995	55.4902	27.66	0.5136	173,117.863	2.2784
CoEr <sub>0.020</sub> Fe <sub>1.980</sub> O <sub>4</sub>	8.367	17.73	2993	53.1555	26.83	0.5208	165,723.033	2.1853
CoEr <sub>0.025</sub> Fe <sub>1.975</sub> O <sub>4</sub>	8.386	15.56	2991	49.5845	25.15	0.5240	154,486.957	2.0400
CoEr <sub>0.030</sub> Fe <sub>1.970</sub> O <sub>4</sub>	8.398	14.4	2989	44.8444	22.88	0.5275	139,625.157	1.8480

**Table 5.**  
*The Magnetic Properties of Er-substituted CoFe<sub>2</sub>O<sub>4</sub>.*

cations in ferrite lattice site [33]. Particularly, high magnetic moment (5 μB) ferrite cations were replaced by erbium cations of magnetic moment 7 μB at B sites. In addition, increasing erbium cations may decrease ratio of ferric and ferrous ions at A, B sites thereby decreasing the magnetic exchange interaction between two sites [34] reducing the Msvalue. It was also observed that increase of erbium content reduced value of Hc from 18998 Oe to 18990Oeinitiating the fact that magnetic moment can be changed with low coercive field, hence coercivity variation is in agreement with variation in anisotropy constant. Henceforth, value of anisotropy constant ‘K’ will decrease further which decreases the energy of magnetic domain wall. Remanent magnetization values decreased from 31 emu/g to 22 emu/system supporting soft magnetic nature due to low coercivity in erbium doped cobalt ferrites [35]. **Table 5** indicates decrease in magnetic moment with increased erbium content which may be assigned to more probable chance of erbium cations to occupy B sites. As per the revealed data increasing erbium content decrease magnetization converting the sample into soft magnetic material. It is understood that increase in erbium content decreases value of ‘K’. M–H loops indicated that soft magnetic Co-Er nano ferrites can be easily magnetized and demagnetized. Squareness ratio ( $R = M_r/M_s$ ) was estimated from

$$R = \frac{M_r}{M_s} \tag{22}$$

where  $M_r$  is Remanent magnetization and  $M_s$  is saturation magnetization. Magnetic moment per unit ( $\eta_B$ ) was calculated from [31, 32].

$$n_B = \frac{M_\omega \times M_S}{5585} \tag{23}$$

where  $M_\omega$  are samples molecular weight and saturation magnetization.

K (magnetic anisotropic constant) is related to the  $M_s$  (saturation magnetization) and Hc (magnetic coercivity) [28] by following relation

$$k = \frac{M_S \times H_c}{0.96} \tag{24}$$

**4. Conclusions**

Synthesis and characterization of erbium substituted cobalt ferrites along with conglomeration was done using citrate-gel auto combustion method. Significant



induced effect of Erbium was observed on the structure of crystal structure, dielectric constant, morphology and electrical transport properties of cobalt ferrite material. Copy of secondary  $\text{ErFeO}_3$  along with primary spinel cubic structure occur only for Er-content,  $x = 0.015, 0.020$  and regains its primary spinel structure for Er content  $x = 0.025, 0.030$  while the crystallite size decreased from 20.84 nm–14.40 nm. According to the SEM analysis the growth in grain along with agglomeration form was found for all samples. With the Erbium substitution which is a combined effect of decrease in resistivity. Small polaron hopping as well as thermally activated mobility of charge carriers was operative in CFEO ceramics and confirmed by DC electrical measurements. Observations indicated strong dependence of magnetic properties on Erbium substitution and coercivity varies in accordance with anisotropy constant. The presence of magnetic dipole could be useful for considering the Erbium substituted cobalt ferrites in electromagnetic applications. The studies of  $\text{CoEr}_x\text{Fe}_{2-x}\text{O}_4$  for compositions with cobalt content  $x = 0.0$  to 0.030 with increasing order of  $x = 0.005$  indicated decreasing crystallite size with increasing erbium content and increase in surface area of the particle makes it a good adsorbent. Hence these adsorbents can be used in gas sensors and waste water treatment etc. ...

## Acknowledgements

Thanks to CSIR, New Delhi, India for Research Fellowship (CSIR-JRF). The authors are grateful to the Prof. Syed Rahman, Head Department of Physics, University College of Science, Osmania University Hyderabad for his constant encouragement.

## Author details

Edapalli Sumalatha<sup>1</sup>, Dachepalli Ravinder<sup>1\*</sup>, Nyathani Maramu<sup>2</sup>, Shubha L.N.<sup>3</sup>, Butreddy Ravinder Reddy<sup>2</sup>, Sadhana Katlakunta<sup>2</sup>, Koteswari Gollapudi<sup>1</sup> and Rajender Thota<sup>1</sup>


<sup>1</sup> Department of Physics, Osmania University, Hyderabad, Telangana, India

<sup>2</sup> Department of Physics, University College of Science, Saifabad, Osmania University, Hyderabad, Telangana, India

<sup>3</sup> Department of Electronics, St. Francis College for Women, Begumpet, Telangana, India

\*Address all correspondence to: ravindergupta28@rediffmail.com

## IntechOpen

© 2021 The Author(s). Licensee IntechOpen. This chapter is distributed under the terms of the Creative Commons Attribution License (<http://creativecommons.org/licenses/by/3.0>), which permits unrestricted use, distribution, and reproduction in any medium, provided the original work is properly cited. 

## References

- [1] Habiba AH, Ondeck CL, Chaudhary P, Bockstaller MR, McHenry ME . Evaluation of iron-cobalt/ferrite core-shell nanoparticles for cancer thermotherapy. *Journal of Applied Physics*. 2008; 103:07A307 <https://doi.org/10.1063/1.2830975>
- [2] Song Q, Zhang ZJ. Shape Control and Associated Magnetic Properties of Spinel Cobalt Ferrite Nanocrystals. *J. Am. Chem. Soc.* 2004; 126, 19, 6164–6168 <https://pubs.acs.org/doi/10.1021/ja049931r>
- [3] Vinosha PA, Das SJ. Investigation on the role of pH for the structural, optical and magnetic properties of cobalt ferrite nanoparticles and its effect on the photo-fenton activity. *Materials Today: Proceedings* 2018;5:8662-8671 <https://www.sciencedirect.com/science/article/pii/S2214785317332807>
- [4] Vázquez-Vázquez C, Lovelle M, Mateo C, López-Quintela MA, Buján-Núñez MC, Serantes D, Baldomir D, Rivas J Magnetocaloric effect and size-dependent study of the magnetic properties of cobalt ferrite nanoparticles prepared by solvothermal synthesis. *Wiley Online Library*: 2008; 205: 1358-1362 <https://doi.org/10.1002/pssa.200778128>
- [5] Nlebedim IC, Hadimani RL, Prozorov R, Jiles DC. Structural, magnetic, and magnetoelastic properties of magnesium substituted cobalt ferrite. *Journal of Applied Physics* 2013; 113: 17A928 <https://doi.org/10.1063/1.4798822>
- [6] Prathapani S, Jayaraman TV, araprasadarao EK, Das D Structural and ambient/sub-ambient temperature magnetic properties of Er-substituted cobalt-ferrites synthesized by sol-gel assisted auto-combustion method, *Journal of Applied Physics*. *Journal of Applied Physics*, 2014;116:023908 <https://doi.org/10.1063/1.4889929>
- [7] Cullity BD, Graham CD *Introduction to Magnetic Materials*, 2nd Edition. Wiley-IEEE Press, 2009;568 Pages <https://www.wiley.com/en-in/Introduction+to+Magnetic+Materials%2C+2nd+Edition-p-9780471477419>
- [8] A. Sathiya Priya, D. Geetha, N. Kavitha, Effect of Al substitution on the structural, electric and impedance behavior of cobalt ferrite, *Vacuum*, 2019, Volume 160, Pages 453-460. <https://doi.org/10.1016/j.vacuum.2018.12.004>.
- [9] Nasir Amin, Muhammad Sajjad Ul Hasan, Zahid Majeed, Zartashia Latif, Muhammad Ajaz un Nabi, Khalid Mahmood, Adnan Ali, Kiran Mehmood, Muneeba Fatima, Maria Akhtar, Muhammad Imran Arshad, Aisha Bibi, Muhammad Zahir Iqbal, Farukh Jabeen, N. Bano, Structural, electrical, optical and dielectric properties of yttrium substituted cadmium ferrites prepared by Co-Precipitation method, *Ceramics International*, 2020, Volume 46, Issue 13, Pages 20798-20809. <https://doi.org/10.1016/j.ceramint.2020.05.079>.
- [10] Salma Aman, Naseeb Ahmad, M.H. Alhossainy, Hind Albalawi, Manal Morsi, Tahani I. Al-Muhimeed, Abeer A. AlObaid, Structural, Magnetic, Electrical and Microwave properties of Spinel Ferrites, *Journal of Rare Earths*, 2021, 1002-0721, <https://doi.org/10.1016/j.jre.2021.04.015>.
- [11] Weiss A (1975) Craik (Ed.) DJ, *Magnetic Oxides*, Parts 1 and 2 (John Wiley & Sons, Bristol, 1975). *Wiley Online Library*, 1975;80:175-175 <https://doi.org/10.1002/bbpc.19760800218>
- [12] Heiba ZK, Mohamed MB, Arda L, Dogan N Cation distribution correlated with magnetic properties of nanocrystalline gadolinium substituted nickel ferrite. *Journal of Magnetism and Magnetic Materials*, 2015; 391:195-202

<https://doi.org/10.1016/j.jmmm.2015.05.003>

[13] Kambale RC, Shaikh PA, Kamble SS, Kolekar YD, Effect of cobalt substitution on structural, magnetic and electric properties of nickel ferrite. *Journal of Alloys and Compounds*, 2009; 478:599-603 <https://www.sciencedirect.com/science/article/abs/pii/S0925838808021257>

[14] Dobrott RD Elements of X-ray Diffraction, Addison-Wesley, London. Characterization of Solid Surfaces, 1959;pp:147-178 [https://link.springer.com/chapter/10.1007/978-1-4613-4490-2\\_8](https://link.springer.com/chapter/10.1007/978-1-4613-4490-2_8)

[15] Andreu I, Natividad E, Ravagli C, Castroa M, Baldib G Heating ability of cobalt ferritenanoparticles showing dynamic and interaction effects. *RSC Adv.*, 2014,4, 28968-28977 <https://doi.org/10.1039/C4RA02586E>

[16] Kakade SG, Ma Y, Devan RS, Kolekar YD, Ramana CV, Dielectric, Complex Impedance, and Electrical Transport Properties of Erbium (Er<sup>3+</sup>) Ion-Substituted Nanocrystalline Cobalt-Rich Ferrite. *J. Phys. Chem. C* 2016, 120, 10, 5682–5693 <https://pubs.acs.org/doi/abs/10.1021/acs.jpcc.5b11188>

[17] Park K, Hwang HK Fabrication and electrical properties of nanocrystalline Dy<sup>3+</sup>-doped CeO<sub>2</sub> for intermediate-temperature solid oxide fuel cells. *Energy*, 2013; 55:304-309 <https://doi.org/10.1016/j.energy.2013.04.017>

[18] Kumar H, Singh JP, Srivastava RC, Negi P, Agrawal HM, Asokan K FTIR and electrical study of dysprosium doped cobalt ferrite nanoparticles, 2014. <https://doi.org/10.1155/2014/862415>

[19] Hashim M, Alimuiddin, Kumar S, Shirsath SE, Kotnala RK, Shah J, Kumar R synthesis and characterization of nickel substuded cobalt ferrite. *Materials Chemistry and Physics*, 2012;

139:364-374 <https://doi.org/10.1016/j.matchemphys.2012.09.019>

[20] Wu Y, Li J, Bai H, He S, Hong Y, Shi K, Zhou Z Colossal Dielectric Behavior and Dielectric Relaxation of (Li, Fe) Co-Doped ZnO Ceramics. *Wiley Online Library:Rapid Research Letter* 2018; 12:1800126 <https://onlinelibrary.wiley.com/doi/abs/10.1002/pssr.201800126>

[21] Salunkhe AB, Khot VM, Phadatare MR, Thorat ND, Joshi RS, Yadav HM, Pawar SH, Low temperature combustion synthesis and magnetostructural properties of CoMnnano-ferrites. *Journal of Magnetism and Magnetic Materials*, 2013; 352:91-98 <https://doi.org/10.1016/j.jmmm.2013.09.020>

[22] Rus SF, Vlazan P, Herklotz A Synthesis and characterization of Zirconium substituted cobalt ferrite nanopowders. *Journal of Nanoscience and Nanotechnology* 2016;16:1 <https://www.osti.gov/pages/servlets/purl/1324165>

[23] Rathore D, Kurchania R, Pandey RK Influence of particle size and temperature on the dielectric properties of CoFe<sub>2</sub>O<sub>4</sub> nanoparticles. *International Journal of Minerals, Metallurgy, and Materials*, 2014; 21:408–414 <https://link.springer.com/article/10.1007/s12613-014-0923-8>

[24] Rahman MT, Ramana CV ( ) Impedance spectroscopic characterization of gadolinium substituted cobalt ferrite ceramics. *Journal of Applied Physics*, 2014;116: 164108 <https://doi.org/10.1063/1.4896945>

[25] Goldman A Modern Ferrite Technology, 2nd ed. Ferrite Technology Pittsburgh, PA, USA 2006. <https://download.e-bookshelf.de/download/0000/0009/50/L-G-0000000950-0002340313.pdf>

- [26] Raghasudha M, Ravinder D, Veerasomaiah P FTIR Studies and Dielectric Properties of Cr Substituted Cobalt Nano Ferrites Synthesized by Citrate-Gel Method. *Nanoscience and Nanotechnology* 2013, 3(5): 105-114 [https://www.researchgate.net/publication/271907985\\_FTIR\\_Studies\\_and\\_Dielectric\\_Properties\\_of\\_Cr\\_Substituted\\_Cobalt\\_Nano\\_Ferrites\\_Synthesized\\_by\\_Citrate-Gel\\_Method](https://www.researchgate.net/publication/271907985_FTIR_Studies_and_Dielectric_Properties_of_Cr_Substituted_Cobalt_Nano_Ferrites_Synthesized_by_Citrate-Gel_Method)
- [27] Kurlyandskaya GV, Bhagat SM, Jacobo SE, esteguy JC, Schegoleva NN, Microwave resonant and zero-field absorption studies of pure and doped cobalt ferrite. *Journal of Physics and Chemistry of Solids* 2011;72:276-285 <https://www.sciencedirect.com/science/article/abs/pii/S0022369711000126?via%3Dihub>
- [28] Kumari N, Kour S, Singh G, Sharma RK A brief review on synthesis, properties and applications of ferrites. *AIP Conference Proceedings*, 2020; 2220:020164 <https://aip.scitation.org/doi/10.1063/5.0001323>
- [29] Pradeep A, Priyadharsini P, Chandrasekaran G, Sol-gel route of synthesis of nanoparticles of MgFe<sub>2</sub>O<sub>4</sub> and XRD, FTIR and VSM study. *Journal of Magnetism and Magnetic Materials* 2008;320:2774-2779 <https://www.sciencedirect.com/science/article/abs/pii/S0304885308007026>
- [30] Mazen SA, Abu-Elsaad NI IR Spectra, Elastic and Dielectric Properties of Li-Mn Ferrite. *International Scholarly Research Notices*, 2012:9 <https://www.hindawi.com/journals/isrn/2012/907257/>
- [31] Kadam AA, Shinde SS, Yadav SP, Patil PS, Rajpure KY Structural, morphological, electrical and magnetic properties of Dy doped Ni-Co substitutional spinel ferrite. *Journal of Magnetism and Magnetic Materials*, 2013; 329:59-64 <https://www.sciencedirect.com/science/article/abs/pii/S030488531200830X>
- [32] Ateia EE, Abdelmaksoud MK, Arman MM, Shafaay AS Comparative study on the physical properties of rare-earth-substituted nano-sized CoFe<sub>2</sub>O<sub>4</sub>. *Applied Physics A*, 2020; 126:91 [https://scholar.cu.edu.eg/sites/default/files/drebtasam/files/comparative\\_.pdf](https://scholar.cu.edu.eg/sites/default/files/drebtasam/files/comparative_.pdf)
- [33] Nag S, Roychowdhury A, Das D, Das S, Mukherjee S Structural and magnetic properties of erbium (Er<sup>3+</sup>) doped nickel zinc ferrite prepared by sol-gel auto-combustion method. *Journal of Magnetism and Magnetic Materials*, 2018; 466:172-179 <https://www.sciencedirect.com/science/article/abs/pii/S0304885317311472>
- [34] Pradeep A, Priyadharsini P, Chandrasekaran G Sol-gel route of synthesis of nanoparticles of MgFe<sub>2</sub>O<sub>4</sub> and XRD, FTIR and VSM study. *Journal of Magnetism and Magnetic Materials*, 2008; 320:2774-2779 <https://www.sciencedirect.com/science/article/abs/pii/S0304885308007026>
- [35] Gabal MA ( ) Magnetic properties of NiCuZn ferrite nanoparticles synthesized using egg-white. *Materials Research Bulletin*, 2010; 45:589-593 <https://www.sciencedirect.com/science/article/abs/pii/S0025540810000279>